

# THE ACHILLES’ HEEL OF LLMS: HOW ALTERING A HANDFUL OF NEURONS CAN CRIPPLE LANGUAGE ABILITIES

Zixuan Qin<sup>1</sup>, Kunlin Lyu<sup>1</sup>, Qingchen Yu<sup>2,3</sup>, Yifan Sun<sup>1\*</sup>, Zhaoxin Fan<sup>2,3†</sup>

<sup>1</sup>Center for Applied Statistics, School of Statistics, Renmin University of China

<sup>2</sup>Beijing Advanced Innovation Center for Future Blockchain and Privacy Computing

<sup>3</sup>School of Artificial Intelligence, Beihang University

## ABSTRACT

Large Language Models (LLMs) have become foundational tools in natural language processing, powering a wide range of applications and research. Many studies have shown that LLMs share significant similarities with the human brain. Recent neuroscience research has found that a small subset of biological neurons in the human brain are crucial for core cognitive functions, which raises a fundamental question: do LLMs also contain a small subset of critical neurons? In this paper, we investigate this question by proposing a Perturbation-based Causal Identification of Critical Neurons method to systematically locate such critical neurons in LLMs. Our findings reveal three key insights: (1) LLMs contain ultra-sparse critical neuron sets. Disrupting these critical neurons can cause a 72B-parameter model with over 1.1 billion neurons to completely collapse, with perplexity increasing by up to 20 orders of magnitude; (2) These critical neurons are not uniformly distributed, but tend to concentrate in the outer layers, particularly within the MLP down\_proj components; (3) Performance degradation exhibits sharp phase transitions, rather than a gradual decline, when these critical neurons are disrupted. Through comprehensive experiments across diverse model architectures and scales, we provide deeper analysis of these phenomena and their implications for LLM robustness and interpretability. These findings can offer guidance for developing more robust model architectures and improving deployment security in safety-critical applications.

## 1 INTRODUCTION

Understanding the fundamental principles underlying intelligent computation has long attracted researchers across neuroscience and artificial intelligence. A growing body of evidence suggests that the brain’s computational power may critically depend on a small fraction of highly influential neurons, rather than being uniformly distributed across all neural elements. This principle, first stated by Arshavsky (2001), suggests that sparsely distributed, genetically distinct neurons function as computational bottlenecks, each having a major influence over specific brain functions.

Recent studies have provided support for this hypothesis across multiple neural systems (Meissner-Bernard et al., 2025; Fan et al., 2025). In the hippocampus, researchers have found small groups of neurons that work together during specific brain events. The neuron groups show precise timing when they activate together. When disrupting these critical neuron groups, memory formation becomes severely impaired, though these groups represent only a tiny fraction of all neurons in the brain (Kunz et al., 2024). Similarly, in sensory cortex, sparse neurons using predictive coding mechanisms prove essential for efficient per-

\*Project leader and Corresponding author. Email: sunyifan@ruc.edu.cn

†Project leader and Corresponding author. Email: zhaoxinf@buaa.edu.cn

ception, with their dysfunction causing pathological states including epileptic activity (Chalk et al., 2018). Motor systems show the same pattern of dependency on sparse neurons. Brief activation patterns in small neuron groups control complex movement sequences. When researchers silence these groups, immediate motor problems occur (Zhang et al., 2024). These findings together suggest that biological neural networks operate under a “sparse criticality” principle, where cognitive and behavioral functions depend critically on the coordinated activity of a minority of highly influential neurons.

In parallel, Large Language Models (LLMs)—with their billions of parameters—have demonstrated capabilities mirroring human cognition, from language comprehension to problem-solving (Riztha et al., 2024; Niu et al., 2024). Recent research shows clear parallels: the hierarchical processing and predictive coding mechanisms in LLMs align closely with the brain’s layered neural architectures (Schrumpf et al., 2021; Caucheteux & King, 2022; Mischnler et al., 2024), hinting that these artificial systems may emulate biological computation. This observation leads to a key question:

**Q: Do LLMs likewise possess a small set of critical artificial neurons that are indispensable for their capabilities?**

In neuroscience, the causal necessity of specific neurons for a given function is often established through lesion studies, which assess behavioral changes following the removal or deactivation of targeted brain regions (Vaidya et al., 2019). Inspired by this classic experimental approach, we ask whether LLMs also show a comparable “critical neuron” phenomenon. To explore this possibility, we similarly adapt the logic of lesion studies to LLMs: since the core function of an LLM is to transform input text into meaningful output for natural language processing tasks (Qin et al., 2024; Zhao et al., 2025), we need to examine the quality and coherence of model outputs after deactivating specific neurons.

To put this investigation into practice, we introduce the Perturbation-based Causal Identification of Critical Neurons method, as illustrated in Figure 1. Given any text as input, the proposed method consists of a two stage optimization process that mirrors the spirit of lesion studies to locate the so called critical neurons. In the first stage, the method injects controlled noise into the model’s input and measures the resulting activation differences across neurons, thereby generating a ranked list of candidates most likely to influence model behavior. In the second

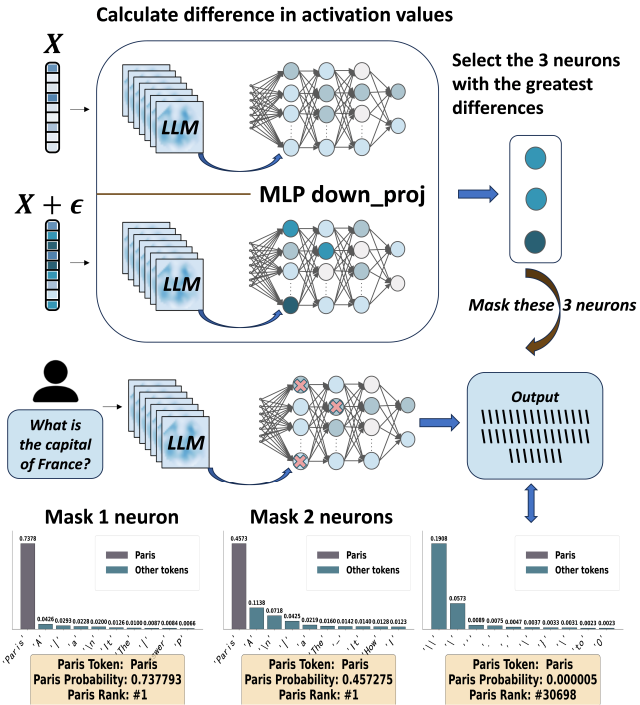


Figure 1: Illustration of critical neuron identification and progressive masking effects, using DeepSeek-R1-Distill-Llama-70B as an example. The top panel shows that our method identifies 3 critical neurons located in MLP down\_proj components of the transformer architecture. The bottom panel demonstrates the progressive degradation of model performance on the question “What is the capital of France?” through sequential masking: the left chart shows token probabilities after masking the first critical neuron, the middle chart shows the effect of masking the first two critical neurons, and the right chart reveals catastrophic failure after masking all three critical neurons. The progression illustrates a sharp phase transition where masking the complete critical neuron set triggers sudden collapse rather than gradual degradation.

stage, we sequentially mask these top-ranked neurons in a greedy manner, closely monitoring changes in model perplexity. This allows us to causally determine which neurons are truly essential for the model’s function.

Using this method, we analyze a diverse set of datasets—including Neurons, WikiText-103, C4, MMLU-Pro (Wang et al., 2025), IFEval (Zhou et al., 2023), GPQA-Diamond (Rein et al., 2024), HumanEval (Peng et al., 2024), MATH (Manem et al., 2025), MGSM (Shi et al., 2023), and SimpleQA (Wei et al., 2024)—as well as multiple LLMs such as Llama-3 (Grattafiori et al., 2024), Gemma (Gemma Team, 2024), DeepSeek-R1 (DeepSeek-AI, 2025), Phi-3, Phi-3.5 (Abdin et al., 2024), and Qwen2.5 (Qwen, 2025). According to our experiment, we observe consistent and interesting patterns across all settings. In particular, our findings reveal several key phenomena. First, we discover that LLMs are governed by an ultra-sparse set of critical neurons: astonishingly, disabling as few as three neurons can catastrophically impair a 72B-parameter model comprising over 1.1 billion neurons, driving its perplexity up by as much as 20 orders of magnitude. Second, we find that these critical neurons are not randomly distributed throughout the network, but are instead highly concentrated in the outer layers, particularly within the MLP down\_proj components, which is consistent with the observations reported in Yu et al. (2025). Third, we observe that performance degradation does not occur gradually, but rather through sharp phase transitions. In section 4, we provide a detailed discussion of these findings and hope these discoveries can help the community better optimize LLM architecture, training, and inference processes. Our contributions are summarized as follows:

- Inspired by lesion studies in neuroscience, we propose a systematic method that integrates noise-based sensitivity analysis with causal verification, which enables us precisely to identify critical neurons that are indispensable for the overall functionality of LLMs. Our method shows exceptional robustness, consistently identifying identical critical neurons for any input texts exceeding a minimum token length threshold ( $T > 10$ ).
- Our analysis uncovers several surprising findings: (a) model performance is predominantly governed by a remarkably small subset of critical neurons; (b) these crucial neurons tend to cluster within specific outer-layer MLP components; and (c) performance degradation exhibits sharp phase transitions if we drop these neurons, rather than a gradual decline, when these critical neurons are disrupted.
- We conduct comprehensive experiments across 21 models ranging from 0.5B to 72B parameters, spanning multiple architecture families and evaluated on diverse datasets including WikiText-103, C4, and seven downstream benchmarks. Across all these varied experimental conditions, our results demonstrate remarkable consistency, with identical critical neuron patterns emerging regardless of model scale, architecture design, or evaluation dataset. This high degree of consistency across such extensive and diverse experimental settings shows the fundamental and universal nature of critical neurons in LLMs.

## 2 RELATED WORK

**Critical Components Analysis in LLMs.** Recent research has revealed a variety of vulnerabilities in LLMs, but most studies have focused on parameter-level rather than neuron-level analysis. For example, Kovaleva et al. (2021) investigates weight outliers in LLMs and finds that anomalous parameters arising during pre-training can significantly affect performance when disabled. Bondarenko et al. (2021) explores activation outliers that influence attention mechanisms, particularly in processing special tokens. Sun et al. (2024) uncovers persistent, large-scale activation patterns at fixed positions across transformer layers, and Yang et al. (2024) attributes such phenomena to architectural components like gated linear units. At the same time, studies on “super weights” show that individual parameters in MLP down\_proj layers can catastrophically impact model performance (Yu et al., 2025), though this line of work mainly addresses quantization rather than systematic vulnerability analysis. While these works together reveal important architectural sensitivities and suggest the existence of critical neurons, they fall short in two key aspects: first, there is still a lack of effective methods for accurately identifying these key neurons; second, systematic analy-

sis of their properties and roles within the model remains unexplored. Our work addresses these limitations by proposing approaches to locate critical neurons and by conducting a comprehensive analysis of their functions across diverse model architectures and scales.

**Neurons Localization and Editing.** Recent studies have advanced neuron-level localization and editing in LLMs, showing that neural parameters can be divided between pattern learning and memorization (Bender et al., 2021). Targeted interventions on specific neurons or clusters enable systematic modification of factual knowledge (Meng et al., 2022; Dai et al., 2022; Li et al., 2024), control of personal information memorization (Chen et al., 2024), multilingual capabilities (Tang et al., 2024), and even safety constraints (Zhou et al., 2025). Further, behavioral attributes such as “aggression” can be manipulated by localizing and editing a small set of neurons (Lee et al., 2025), and polysemantic neurons in fusion heads are linked to modality collapse in multimodal models (Chaudhuri et al., 2025). However, existing work primarily focuses on task-specific interventions, lacking systematic frameworks for identifying neurons critical to core model functionality. Our work addresses this gap by introducing a principled method for neuron localization and causal verification, inspired by lesion studies in neuroscience.

### 3 METHODOLOGY

This paper aims to define and address the problem of identifying **critical neurons** in LLMs. The central question is: *Which neurons are essential for the model’s performance, such that their removal causes substantial degradation?* Identifying such neurons enables us to better understand model internals and analyze the consequences of their ablation.

Formally, let  $N$  denote the set of all neurons in the model. Our goal is to find a sparse subset  $S^* \subseteq N$  (with  $|S^*| \ll |N|$ ) such that masking these neurons results in a significant drop in model performance, as measured by a predefined degradation threshold  $\epsilon$ .

To operationalize this, we apply a neuron masking protocol: for any neuron  $(l, i)$  at layer  $l$  and index  $i$ , we define its activation under masking as

$$\tilde{n}_l^{(i)}(\mathbf{x}) = \begin{cases} 0 & \text{if } (l, i) \in S \\ n_l^{(i)}(\mathbf{x}) & \text{otherwise} \end{cases} \quad (1)$$

where  $S$  is the set of masked neurons. Let  $M^{-S}$  denote the model with neurons in  $S$  masked.

We quantify the impact of masking via the change in perplexity (Appendix A.1) given a sequence of data an input:

$$\Delta(\mathbf{x}, S) = \log_{10} \left( \frac{\text{PPL}_{M^{-S}}(\mathbf{x})}{\text{PPL}_M(\mathbf{x})} \right) = \frac{1}{T \ln 10} \sum_{t=1}^T [\log P_M(x_t | \mathbf{x}_{<t}) - \log P_{M^{-S}}(x_t | \mathbf{x}_{<t})] \quad (2)$$

where  $T$  is the sequence length, PPL denotes perplexity, and  $P_M$  is the predicted token probability.

The critical neuron identification problem is thus:

*Given a model  $M$  and input  $\mathbf{x}$ , find the minimal neuron set  $S^* \subseteq N$  such that  $\Delta(\mathbf{x}, S^*) \geq \epsilon$ .*

After identifying  $S^*$ , we can further analyze the effects of masking these neurons to understand their functional roles and contributions to model behavior. To solve the problem, building on the mathematical framework established in Appendix A.1, we propose a method, which operationalizes the theoretical definitions through a two-stage process: (1) neuron importance quantification via sensitivity analysis, and (2) causal verification of criticality through systematic masking interventions. Next, we introduce each stage in detail. Additional computational efficiency analysis and algorithmic implementations are provided in Appendix A.2.

**Stage 1: Neuron Importance Evaluation.** The first stage establishes neuron ranking based on sensitivity to input perturbations. Given input text  $p$  and model  $f_\theta$ , we embed  $p$  into sequence  $\mathbf{x}$ , and employ Monte Carlo sampling with  $K$  iterations to estimate each

neuron’s importance. In each iteration  $i$ , we generate a perturbed input  $\tilde{\mathbf{x}}_i = \mathbf{x} + \alpha \cdot \epsilon_i$  where  $\epsilon_i \sim \mathcal{N}(\mathbf{0}, \mathbf{I})$  represents Gaussian noise and  $\alpha$  controls the perturbation magnitude. We then compute the noisy activation  $A_i^{\text{noisy}} = f_\theta(\tilde{\mathbf{x}}_i)$  and compare it with the clean activation  $A_i^{\text{clean}} = f_\theta(\mathbf{x})$ .

For each neuron  $s$ , we iteratively accumulate the activation differences across all  $K$  perturbations to compute the importance score:

$$\text{Imp}(s) = \frac{1}{K} \sum_{i=1}^K |A_s^{\text{clean}} - A_{i,s}^{\text{noisy}}| \xrightarrow{K \rightarrow \infty} \mathbb{E}_{\epsilon \sim \mathcal{N}(\mathbf{0}, \mathbf{I})} [|f_{\theta,s}(\mathbf{x}) - f_{\theta,s}(\mathbf{x} + \alpha \cdot \epsilon)|] \quad (3)$$

By the Law of Large Numbers, this Monte Carlo estimator converges to the true expected sensitivity as  $K$  increases. After computing importance scores for all neurons, we sort them in descending order to obtain the ranked list  $S = \{s_1, s_2, \dots, s_N\}$  where  $\text{Imp}(s_1) \geq \text{Imp}(s_2) \geq \dots \geq \text{Imp}(s_N)$ .

**Stage 2: Critical Neuron Identification.** The second stage solves the optimization problem of finding the minimal critical set. Given the importance-ranked neuron list  $S$  from Stage 1 and threshold  $\epsilon$ , our objective is to find:

$$n^* = \arg \min_n \{n : \Delta(\mathbf{x}, S_n) \geq \epsilon\} \quad \text{where } S_n = \{s_1, s_2, \dots, s_n\} \quad (4)$$

Since exhaustive enumeration of all possible subsets requires  $O(2^{|N|})$  complexity, we leverage our importance ranking to design a greedy search algorithm. Given the sorted neuron list  $S$  and threshold  $\epsilon$  as inputs, we use an iterative greedy search that progressively increases the candidate set size as the iteration variable. Specifically, we iterate over  $n = \Delta n, 2\Delta n, 3\Delta n, \dots$  where  $\Delta n$  is the step size, and in each iteration we update the candidate set  $S_n = \{s_1, s_2, \dots, s_n\}$  to include the top- $n$  highest-ranked neurons from our importance list. For each updated candidate set, we apply the masking operation by setting  $\tilde{n}_l^{(i)}(\mathbf{x}) = 0$  for all neurons  $(l, i) \in S_n$ , then evaluate the resulting masked model  $M^{-S_n}$  to compute the performance degradation  $\Delta(\mathbf{x}, S_n) = \log_{10}(\text{PPL}_{M-S_n}(\mathbf{x}) / \text{PPL}_M(\mathbf{x}))$ . The algorithm terminates when the degradation exceeds our threshold  $\Delta(\mathbf{x}, S_n) \geq \epsilon$ , returning the minimal set  $S_{n^*}$  that causes catastrophic language capability degradation. This greedy approach reduces computational complexity to  $O(|N|)$  by testing only  $\lceil |N| / \Delta n \rceil$  candidate sets rather than all  $2^{|N|}$  possible combinations, while effectively approximating the optimal solution.

Our method only takes one sequence as input for any LLMs, which makes our method extremely robust and reliable (see Section 4 experiment for proof). Under sufficient parameter settings (when  $K$  and  $\alpha$  are adequately large) and for input texts exceeding a minimum token length threshold ( $T > 10$ ), the identified critical neurons remain identical across repeated experiments (details can be found in Section 4.4).

## 4 EXPERIMENTS

### 4.1 EXPERIMENTAL SETUP

**Datasets.** We conduct our investigation across multiple datasets to assess both language modeling capabilities and downstream task performance. For language modeling, we primarily use WikiText-103 and the C4 dataset. To evaluate the impact of critical neuron masking on specific capabilities, we employ seven additional benchmarks: MMLU Pro (Wang et al., 2025) for advanced multi-domain knowledge, IFEval (Zhou et al., 2023) for instruction following, GPQA Diamond (Rein et al., 2024) for graduate-level scientific reasoning, HumanEval (Peng et al., 2024) for code generation, MATH (Manem et al., 2025) for mathematical problem solving, SimpleQA (Wei et al., 2024) for factual question answering, and MGSM (Shi et al., 2023) for multilingual mathematical reasoning. Detailed evaluation protocols and metrics for each benchmark are provided in Appendix A.3.

**Implementation Details.** We follow the methodology described in Section 3, with parameter configurations chosen to balance accuracy and computational efficiency. For input perturbation, we set the noise scale to  $\alpha = 5$  and randomly generate  $K = 100$  noisy samples for neuron importance evaluation. A greedy search with step size  $\Delta n = 1$  and criticality threshold  $\epsilon = 1$  is used throughout our analysis (see Appendix A.4). For each experiment, we use a consistent input text  $p$ : "Later reviews were more positive..." - a 30-token Wikipedia text that ensures standardized evaluation conditions across all models. All experiments are conducted on a high-performance computing cluster equipped with 4 NVIDIA A800 GPUs (80GB each). We use PyTorch (Paszke et al., 2019) and employ mixed-precision (fp16) for efficient memory utilization and faster inference. Model loading and inference are fully automated using standardized scripts. Our experimental evaluation is structured around three core components: (1) A comprehensive analysis revealing the existence, distribution, and failure patterns of ultra-sparse critical neurons across all models; (2) Comparison studies benchmarking our method against alternative neuron location strategies; (3) Ablation study assessing the robustness of our critical neuron localization algorithm. Extensive results validate our key findings regarding critical neuron vulnerabilities in modern LLMs.

## 4.2 INVESTIGATION RESULTS

Our investigation covers 21 LLMs spanning diverse architectures and parameter scales (0.5B–72B), including the Llama-3, Gemma, DeepSeek-R1-Distill, Phi-3, and Qwen2.5 families (Grattafiori et al., 2024; Qwen, 2025; DeepSeek-AI, 2025; Gemma Team, 2024; Abdin et al., 2024), and we conduct evaluations using multiple datasets. This investigation enables a systematic assessment of neuron criticality across a broad range of model architectures and parameter scales. Our investigation leads to the following three key findings. Next, we analyze the three findings in detail.

### Key Findings

**Finding 1:** Disrupting as few as three ultra-sparse critical neurons can catastrophically impair LLM capabilities; for example, masking just 3 out of over 1.1 billion neurons in a 72B-parameter model leads to a complete collapse, with perplexity increasing by up to 20 orders of magnitude.

**Finding 2:** Critical neurons are unevenly distributed across the network, exhibiting a strong tendency to cluster in the outer layers, particularly within MLP `down_proj` components.

**Finding 3:** Performance degradation manifests as sharp phase transitions rather than gradual declines when these critical neurons are disrupted.

**Ultra-Sparse Vulnerability: Three Neurons Can Collapse Billion-Parameter Models.** We observe an extraordinary phenomenon across all tested LLMs: the existence of ultra-sparse critical neuron sets whose disruption leads to catastrophic system failure. Table 1 presents comprehensive experimental results across 21 models, demonstrating that merely 3 neurons can catastrophically compromise models containing billions of parameters, with neuron rates consistently falling in the  $10^{-8}$  range. Masking 3 neurons in Gemma-7B increases WikiText-103 perplexity from 9.98 to  $6.25 \times 10^{21}$ —a staggering 20 orders of magnitude increase. Our method exhibits perfect consistency across experimental conditions: for any given LLM, we identify the exact same critical neurons regardless of input text, confirming these are intrinsic architectural dependencies. This pattern aligns with established neuroscience principles (Arshavsky, 2001), showing that LLMs also rely heavily on sparse, highly influential neurons as computational bottlenecks. Examples of model responses before and after critical neuron masking are provided in Appendix A.5.

Table 2 documents the impact of critical neuron masking on seven diverse benchmark tasks across three representative 70B models. The results reveal that critical neuron masking triggers comprehensive collapse across all downstream capabilities, extending beyond language modeling degradation to complete task failure across diverse domains. Models achieve zero performance on knowledge retrieval (MMLU Pro (Wang et al., 2025)), reasoning (GPQA Di-

Table 1: Critical neuron masking results across 21 LLMs. For each model, we report the minimal number of critical neurons required to induce catastrophic performance degradation and the neuron rate as a fraction of total neurons. Original and Masked columns show perplexity values before and after masking critical neurons on WikiText-103 and C4 datasets.

Model Family	Model	Critical Neurons Number	Critical Neurons Rate ( $10^{-8}$ )	WikiText-103 Original → Masked	C4 Original → Masked
Llama-3	Llama-3.2-1B-Instruct	4	6.43	$17.74 \rightarrow 1.58 \times 10^6$	$21.15 \rightarrow 1.41 \times 10^6$
	Llama-3.2-3B-Instruct	4	3.19	$13.36 \rightarrow 3.79 \times 10^5$	$16.47 \rightarrow 4.69 \times 10^5$
	Llama-3.8B-Instruct	5	2.21	$10.88 \rightarrow 1.48 \times 10^6$	$14.04 \rightarrow 1.01 \times 10^6$
	Llama-3.3-70B-Instruct	7	0.63	$5.41 \rightarrow 3.86 \times 10^6$	$8.65 \rightarrow 2.18 \times 10^6$
Gemma	Gemma-2B	9	7.79	$12.58 \rightarrow 2.36 \times 10^{16}$	$13.59 \rightarrow 6.66 \times 10^{15}$
	Gemma-7B	3	1.01	$9.98 \rightarrow 6.25 \times 10^{21}$	$11.41 \rightarrow 1.32 \times 10^{20}$
DeepSeek-R1	DeepSeek-R1-Distill-Qwen-1.5B	23	21.12	$61.05 \rightarrow 1.28 \times 10^3$	$49.09 \rightarrow 1.19 \times 10^3$
	DeepSeek-R1-Distill-Qwen-7B	3	1.28	$34.57 \rightarrow 5.59 \times 10^3$	$35.62 \rightarrow 3.70 \times 10^3$
	DeepSeek-R1-Distill-Llama-8B	3	1.33	$17.56 \rightarrow 2.81 \times 10^5$	$23.43 \rightarrow 2.55 \times 10^5$
	DeepSeek-R1-Distill-Qwen-14B	4	1.12	$12.85 \rightarrow 6.85 \times 10^3$	$19.26 \rightarrow 5.00 \times 10^3$
	DeepSeek-R1-Distill-Qwen-32B	28	3.58	$9.36 \rightarrow 8.07 \times 10^2$	$15.14 \rightarrow 7.40 \times 10^2$
	DeepSeek-R1-Distill-Llama-70B	3	0.27	$7.86 \rightarrow 2.21 \times 10^4$	$11.34 \rightarrow 1.84 \times 10^4$
Phi-3	Phi-3-mini-4k-Instruct	13	6.83	$8.24 \rightarrow 9.51 \times 10^4$	$10.57 \rightarrow 4.69 \times 10^4$
	Phi-3.5-mini-Instruct	13	6.83	$8.46 \rightarrow 2.67 \times 10^6$	$10.71 \rightarrow 1.02 \times 10^6$
Qwen2.5	Qwen2.5-0.5B-Instruct	3	5.90	$18.18 \rightarrow 1.76 \times 10^6$	$22.34 \rightarrow 1.08 \times 10^6$
	Qwen2.5-1.5B-Instruct	11	10.19	$12.37 \rightarrow 4.01 \times 10^2$	$15.95 \rightarrow 3.28 \times 10^2$
	Qwen2.5-3B-Instruct	5	2.89	$11.24 \rightarrow 3.34 \times 10^3$	$14.28 \rightarrow 2.52 \times 10^3$
	Qwen2.5-7B-Instruct	10	4.30	$9.75 \rightarrow 9.64 \times 10^4$	$13.01 \rightarrow 7.61 \times 10^4$
	Qwen2.5-14B-Instruct	4	1.13	$7.69 \rightarrow 2.39 \times 10^3$	$11.12 \rightarrow 1.59 \times 10^3$
	Qwen2.5-32B-Instruct	45	5.80	$7.40 \rightarrow 1.01 \times 10^2$	$10.98 \rightarrow 0.94 \times 10^2$
	Qwen2.5-72B-Instruct	3	0.26	$10.23 \rightarrow 2.24 \times 10^4$	$10.72 \rightarrow 1.40 \times 10^4$

amond (Rein et al., 2024)), code generation (HumanEval (Peng et al., 2024)), mathematical problem solving (MATH (Manem et al., 2025)), instruction following (IFEval (Zhou et al., 2023)), multilingual reasoning (MGSM (Shi et al., 2023)), and factual question answering (SimpleQA (Wei et al., 2024)). This universal collapse documented in the table confirms that critical neurons control core language processing functions rather than task-specific components. The universal nature of these phenomena across diverse architectures, scales, and datasets suggests fundamental properties of current transformer-based language models rather than implementation artifacts.

Table 2: Impact of critical neuron masking on downstream task performance across three representative 70B models. Performance is measured as accuracy/success rate on each benchmark. Blue shading highlights the complete task failure (0.0000) after masking critical neurons, demonstrating catastrophic capability collapse across all evaluated tasks.

Model	Condition	MMLU-Pro	IFEval	GPQA-Diamond	HumanEval	MATH	MGSM	SimpleQA
Llama-3.3-70B-Instruct	Original	0.4441	0.4658	0.2879	0.2988	0.4420	0.9590	0.3704
	Masked	0.0000	0.0000	0.0000	0.0000	0.0000	0.0000	0.0000
DeepSeek-R1-Distill-Llama-70B	Original	0.1631	0.2458	0.1869	0.1951	0.1420	0.9809	0.3104
	Masked	0.0000	0.0000	0.0000	0.0000	0.0000	0.0000	0.0000
Qwen2.5-72B-Instruct	Original	0.2442	0.5268	0.3687	0.2866	0.3140	0.9080	0.2443
	Masked	0.0000	0.0000	0.0000	0.0000	0.0000	0.0000	0.0000

**Architectural Concentration: Critical Neurons Cluster in Outer Layers and MLP Components.** Our analysis reveals systematic concentration patterns in critical neuron distribution across all tested architectures. Figure 2 illustrates the architectural distribution of critical neurons across six representative models. The figure shows that critical neurons exhibit a clear bias toward outer layers rather than being uniformly distributed throughout the model depth. Furthermore, within these layers, critical neurons mainly reside in MLP down\_proj components, with occasional variations in other architectural elements across different model families. The variations stem from different architectural designs and training procedures across model families. This concentration reflects the information compression role of down\_proj, which transforms high-dimensional representations back to the model’s embedding space. This finding is consistent with (Yu et al., 2025).

This concentration reflects the distinct computational roles of different network depths. Early layers handle fundamental feature extraction, making them critical for establishing the computational foundation. Late layers perform final integration and output generation, serving as bottlenecks for translating representations into responses. Middle layers

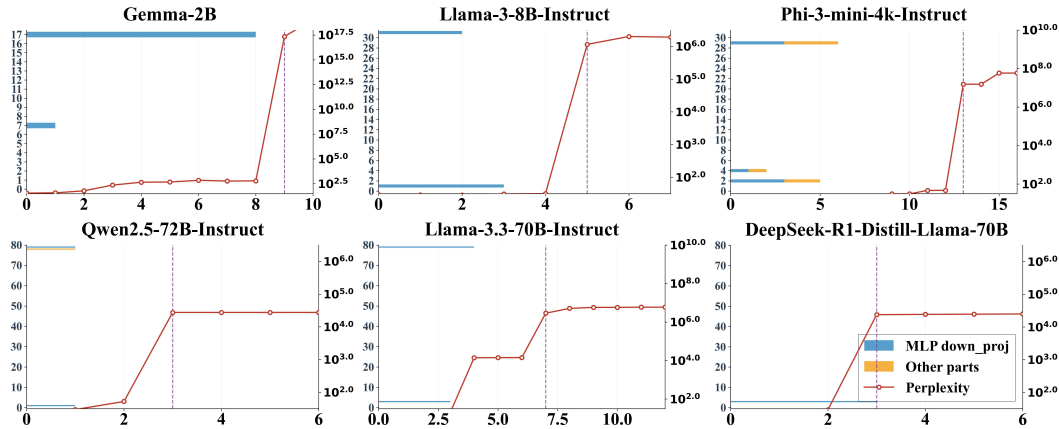


Figure 2: Phase transitions and architectural distribution of critical neurons across six representative models. The figure is organized in a  $2 \times 3$  grid showing different models: top row displays Gemma-2B, Llama-3-8B-Instruct, and Phi-3-mini-4k-Instruct; bottom row shows Qwen2.5-72B-Instruct, Llama-3.3-70B-Instruct, and DeepSeek-R1-Distill-Llama-70B. Each subplot employs a dual-axis design with two distinct visualizations. For the layer distribution analysis (horizontal bars), the x-axis represents layer numbers (ranging from 0 to the maximum number of layers for each model), while the y-axis represents the count of critical neurons found at each layer. Blue bars indicate critical neurons located in MLP down\_proj components, while orange bars represent critical neurons in other architectural components. For the phase transition analysis, the x-axis indicates the number of progressively masked neurons (0 to approximately 10-15 depending on the model), while the right y-axis shows perplexity values. The red curve with circle markers traces the evolution of perplexity as neurons are cumulatively masked in order of importance. Vertical dashed lines mark the critical threshold where sudden performance collapse occurs.

perform step-by-step refinement that can tolerate disruption through redundant pathways (Sun et al., 2025; Bogomasov & Conrad, 2025). MLP down\_proj components in outer layers are particularly vulnerable because they compress high-dimensional representations, creating information bottlenecks. When these compression points fail, information loss spreads throughout the network, causing system-wide collapse.

**Phase Transition Behavior: Sharp Thresholds Trigger Sudden Collapse.** Performance degradation exhibits sharp phase transition behavior rather than gradual decline across all tested models. Figure 2 displays the phase transition behavior of critical neuron masking across six representative models, demonstrating that models maintain near-normal performance while progressively masking neurons, then experience sudden catastrophic collapse when the critical neuron set reaches a threshold size. The visualization reveals that this threshold behavior demonstrates critical neurons function as a collective computational unit rather than individual switches. The curves shown in the figure illustrate that masking individual critical neurons in isolation produces minimal impact on model performance, but when the complete critical neuron set is disrupted together, it triggers sudden system-wide collapse. The phase transition patterns demonstrate that models can tolerate masking several important neurons individually with negligible effects, but simultaneously masking the identified critical neuron set causes explosive perplexity increases spanning multiple orders of magnitude (additional results are provided in Appendix A.6).

The sharp phase transition behavior can be attributed to the highly interdependent nature of information processing in transformer architectures. Critical neurons appear to form a tightly coupled computational circuit where each neuron’s function depends critically on inputs from others within the same set. Individual neuron masking fails to disrupt the circuit because remaining neurons can partially compensate through their shared computational pathways. When multiple critical neurons are simultaneously removed, the circuit loses its functional integrity, creating cascading information bottlenecks that spread throughout the network (Ziyin & Ueda, 2022; Manem et al., 2025).

### 4.3 COMPARISON WITH EXISTING NEURON LOCALIZATION METHODS

To validate the effectiveness of our method, we conduct comparison studies examining different neuron location strategies. We systematically compare our approach against alternative neuron location strategies across three representative 70B models. Our evaluation includes random selection and two importance-based alternatives: activation magnitude (AM) (Sattarifard et al., 2025) ranking and gradient magnitude (GM) (Liu et al., 2025) ranking. We evaluate each strategy by progressively masking neurons from 0 to 1,000 and measuring the perplexity. AM ranks neurons by their activation values, while GM ranks by the magnitude of perplexity gradients with respect to each neuron. For random selection, we average results over 10 trials to ensure statistical reliability.

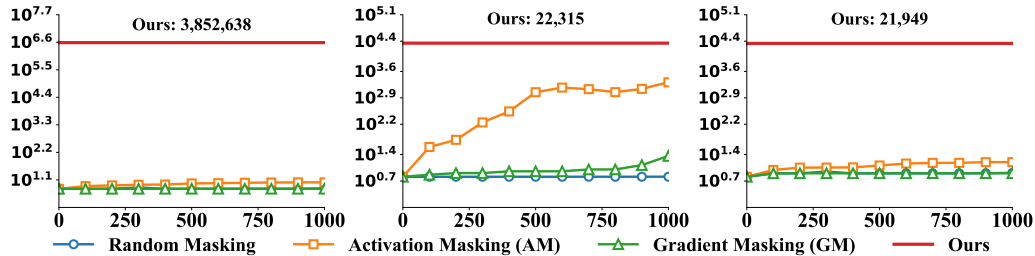


Figure 3: Comparison of neuron location strategies across three 70B models on WikiText-103 (1,000 samples). X-axis shows the number of masked neurons, Y-axis shows perplexity values. Left: Llama-3.3-70B-Instruct, Center: Qwen2.5-72B-Instruct, Right: DeepSeek-R1-Distill-Llama-70B. Random masking (averaged 10 trials) shows gradual perplexity increase. Activation magnitude ranking (AM) demonstrates moderate effectiveness with steeper increases. Gradient magnitude ranking (GM) shows limited degradation that plateaus quickly. Our method represents the catastrophic perplexity achieved by masking minimal critical neurons identified by our approach.

Figure 3 presents a comparison of different neuron selection strategies across three 70B models, revealing that gradient-based and activation-based methods fail to identify critical neurons because they rely on static importance measures that do not capture dynamic sensitivity to input variations. Gradient magnitude reflects importance for specific inputs but cannot generalize across diverse contexts, while activation magnitude indicates computational load rather than functional criticality. The results show that even when masking up to 1,000 neurons, these alternative methods achieve only modest perplexity increases. In contrast, our method identifies ultra-sparse critical sets that cause catastrophic failure. This difference validates the superior precision of our method in identifying neurons that control fundamental language capabilities.

### 4.4 ABLATION STUDY

Our method demonstrates exceptional robustness. Particularly, we demonstrate that for input texts exceeding a minimum token length threshold ( $T > 10$ ), regardless of text types (Wikipedia, news, biography, media) or languages (English, French, German, Chinese, Spanish), the identified critical neurons remain consistent for each model when  $K$  and  $\alpha$  reach stable values ( $K = 100$ ,  $\alpha = 5$ ). Furthermore, we find that models subjected to fine-tuning and reinforcement learning retain the same critical neuron locations, and masking these neurons continues to cause identical catastrophic failures, indicating that these architectural dependencies persist across different training approaches. The token length threshold analysis, detailed cross-linguistic validation results, and fine-tuning robustness experiments are provided in Appendix A.7.

We conduct parameter analysis to examine the stability of our method. Figure 4 shows that the noise scale  $\alpha$  exhibits a clear threshold effect, with fluctuations before  $\alpha = 5$ , then stabilizing consistently at 7 neurons for all values where  $\alpha \geq 5$ . The sample size  $K$  demonstrates different convergence characteristics, showing initial fluctuations at smaller sample sizes but achieving consistent stability at 7 neurons once  $K$  exceeds 80. These convergence patterns reveal that parameters have distinct minimum thresholds:  $\alpha$  requires sufficient perturbation

to effectively distinguish critical neurons from non-critical ones, while  $K$  needs adequate sampling to reduce statistical noise. After carefully balancing computational efficiency and accuracy requirements, we select  $\alpha = 5$  and  $K = 100$  as our standard parameters.

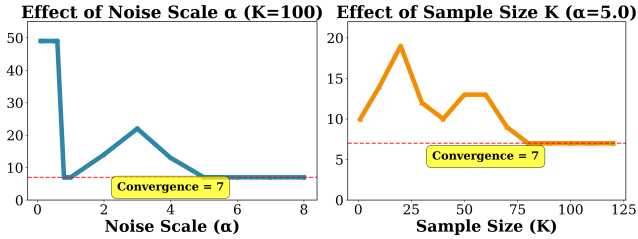


Figure 4: Parameter sensitivity analysis for Llama-3.3-70B-Instruct. Left subplot: x-axis represents noise scale  $\alpha$  (0 to 8), y-axis represents number of critical neurons (0 to 50), blue line shows the relationship with fixed  $K = 100$ . Right subplot: x-axis represents sample size  $K$  (0 to 125), y-axis represents number of critical neurons (0 to 20), orange line shows the relationship with fixed  $\alpha = 5.0$ . Red dashed horizontal lines in both subplots mark the value of 7 neurons.

Additionally, we validate that completely masking critical neurons represents the most effective perturbation strategy compared to alternative scaling approaches. Through analysis of different scaling factors applied to critical neuron activations, we confirm that complete masking produces the maximum performance degradation, justifying our methodological choice (see Appendix A.8).

## 5 CONCLUSION

Despite impressive LLM capabilities, their internal computational structure remains incompletely understood. We present a perturbation-based approach for identifying critical neuron dependencies, applying it to 21 models (0.5B-72B parameters). Our results reveal that model behavior is governed by ultra-sparse neuron subsets, primarily in outer layers and MLP down\_proj components, whose modification causes abrupt performance shifts across all evaluated capabilities.

For future work, we aim to develop a deeper understanding of these findings to formulate effective defensive strategies (see Appendix A.9), and to develop strategies for architectural improvements that more evenly distribute critical computational functions throughout the network.

## REFERENCES

Marah Abdin, Jyoti Aneja, Hany Awadalla, Ahmed Awadallah, Ammar Ahmad Awan, Nguyen Bach, et al. Phi-3 technical report: A highly capable language model locally on your phone, 2024. URL <https://arxiv.org/abs/2404.14219>.

Yuri I. Arshavsky. Role of individual neurons and neural networks in cognitive functioning of the brain: A new insight. *Brain and Cognition*, 46(3):414–428, 2001. ISSN 0278-2626. doi: <https://doi.org/10.1006/brcg.2001.1299>. URL <https://www.sciencedirect.com/science/article/pii/S0278262601912990>.

Emily M. Bender, Timnit Gebru, Angelina McMillan-Major, and Shmargaret Shmitchell. On the dangers of stochastic parrots: Can language models be too big. In *Proceedings of the 2021 ACM Conference on Fairness, Accountability, and Transparency*, FAccT '21, pp. 610–623, New York, NY, USA, 2021. Association for Computing Machinery. ISBN 9781450383097. doi: 10.1145/3442188.3445922. URL <https://doi.org/10.1145/3442188.3445922>.

Sergey Bochkhanov. On sparse connectivity, adversarial robustness, and a novel model of the artificial neuron. In *1st Visual Inductive Priors for Data-Efficient Deep Learning Workshop*, 2020. URL [https://openreview.net/forum?id=S4kvQ7\\_XBxP](https://openreview.net/forum?id=S4kvQ7_XBxP).

Kirill Bogomasov and Stefan Conrad. Exploring the impact of activation functions on vision transformer performance. In *Proceedings of the 2024 8th International Conference on Advances in Artificial Intelligence, ICAAI '24*, pp. 345–350, New York, NY, USA, 2025. Association for Computing Machinery. ISBN 9798400718014. doi: 10.1145/3704137.3704172. URL <https://doi.org/10.1145/3704137.3704172>.

Yelysei Bondarenko, Markus Nagel, and Tijmen Blankevoort. Understanding and overcoming the challenges of efficient transformer quantization. In Marie-Francine Moens, Xuanjing Huang, Lucia Specia, and Scott Wen-tau Yih (eds.), *Proceedings of the 2021 Conference on Empirical Methods in Natural Language Processing*, pp. 7947–7969, Online and Punta Cana, Dominican Republic, November 2021. Association for Computational Linguistics. doi: 10.18653/v1/2021.emnlp-main.627. URL [https://aclanthology.org/2021.emnlp-main.627/](https://aclanthology.org/2021.emnlp-main.627).

Charlotte Caucheteux and Jean-Rémi King. Brains and algorithms partially converge in natural language processing. *Communications Biology*, 5(1):134, 2 2022. ISSN 2399-3642. doi: 10.1038/s42003-022-03036-1. URL <https://doi.org/10.1038/s42003-022-03036-1>.

Matthew Chalk, Olivier Marre, and Gašper Tkačik. Toward a unified theory of efficient, predictive, and sparse coding. *Proceedings of the National Academy of Sciences*, 115(1):186–191, 2018. doi: 10.1073/pnas.1711114115. URL <https://www.pnas.org/doi/abs/10.1073/pnas.1711114115>.

Abhra Chaudhuri, Anjan Dutta, Tu Bui, and Serban Georgescu. A closer look at multimodal representation collapse. In *Forty-second International Conference on Machine Learning*, 2025. URL <https://openreview.net/forum?id=Vf9f7eNX6T>.

Ruizhe Chen, Tianxiang Hu, Yang Feng, and Zuozhu Liu. Learnable privacy neurons localization in language models. In Lun-Wei Ku, Andre Martins, and Vivek Srikumar (eds.), *Proceedings of the 62nd Annual Meeting of the Association for Computational Linguistics (Volume 2: Short Papers)*, pp. 256–264, Bangkok, Thailand, August 2024. Association for Computational Linguistics. doi: 10.18653/v1/2024.acl-short.25. URL <https://aclanthology.org/2024.acl-short.25/>.

Zhuotong Chen, Qianxiao Li, and Zheng Zhang. Towards robust neural networks via close-loop control, 2021. URL <https://arxiv.org/abs/2102.01862>.

Chih-Hong Cheng. Provably-robust runtime monitoring of neuron activation patterns, 2021. URL <https://arxiv.org/abs/2011.11959>.

Chih-Hong Cheng, Georg Nührenberg, and Hirotoshi Yasuoka. Runtime monitoring neuron activation patterns, 2018. URL <https://arxiv.org/abs/1809.06573>.

Damai Dai, Li Dong, Yaru Hao, Zhifang Sui, Baobao Chang, and Furu Wei. Knowledge neurons in pretrained transformers. In Smaranda Muresan, Preslav Nakov, and Aline Villavicencio (eds.), *Proceedings of the 60th Annual Meeting of the Association for Computational Linguistics (Volume 1: Long Papers)*, pp. 8493–8502, Dublin, Ireland, May 2022. Association for Computational Linguistics. doi: 10.18653/v1/2022.acl-long.581. URL <https://aclanthology.org/2022.acl-long.581/>.

DeepSeek-AI. Deepseek-r1: Incentivizing reasoning capability in llms via reinforcement learning, 2025. URL <https://arxiv.org/abs/2501.12948>.

Liangwei Fan, Hui Shen, Xiangkai Lian, Yulin Li, Man Yao, Guoqi Li, and Dewen Hu. A multisynaptic spiking neuron for simultaneously encoding spatiotemporal dynamics. *Nature Communications*, 16(1):7155, 08 2025. doi: 10.1038/s41467-025-62251-6. URL <https://doi.org/10.1038/s41467-025-62251-6>.

Gemma Team. Gemma: Open models based on gemini research and technology, 2024. URL <https://arxiv.org/abs/2403.08295>.

Aaron Grattafiori, Abhimanyu Dubey, Abhinav Jauhri, et al. The llama 3 herd of models, 2024. URL <https://arxiv.org/abs/2407.21783>.

Alessandra Griffa, Mathieu Mach, Julien Dedelley, Daniel Gutierrez-Barragan, Alessandro Gozzi, Gilles Allali, Joanes Grandjean, Dimitri Van De Ville, and Enrico Amico. Evidence for increased parallel information transmission in human brain networks compared to macaques and male mice. *Nature Communications*, 14(1):8216, 2023. doi: 10.1038/s41467-023-43971-z. URL <https://doi.org/10.1038/s41467-023-43971-z>.

Hanbo Huang, Yihan Li, Bowen Jiang, Lin Liu, Bo Jiang, Ruoyu Sun, Zhuotao Liu, and Shiyu Liang. Position: On-premises llm deployment demands a middle path: Preserving privacy without sacrificing model confidentiality, 2025. URL <https://arxiv.org/abs/2410.11182>.

Nidhal Jegham, Marwan Abdelatti, and Abdeltawab Hendawi. Visual reasoning evaluation of grok, deepseek janus, gemini, qwen, mistral, and chatgpt, 2025. URL <https://arxiv.org/abs/2502.16428>.

Olga Kovaleva, Saurabh Kulshreshtha, Anna Rogers, and Anna Rumshisky. BERT busters: Outlier dimensions that disrupt transformers. In Chengqing Zong, Fei Xia, Wenjie Li, and Roberto Navigli (eds.), *Findings of the Association for Computational Linguistics: ACL-IJCNLP 2021*, pp. 3392–3405, Online, August 2021. Association for Computational Linguistics. doi: 10.18653/v1/2021.findings-acl.300. URL <https://aclanthology.org/2021.findings-acl.300>.

Lukas Kunz, Bernhard P. Staresina, Peter C. Reinacher, Armin Brandt, Tim A. Guth, Andreas Schulze-Bonhage, and Joshua Jacobs. Ripple-locked coactivity of stimulus-specific neurons and human associative memory. *Nature Neuroscience*, 27(3):587–599, 3 2024. ISSN 1546-1726. doi: 10.1038/s41593-023-01550-x. URL <https://doi.org/10.1038/s41593-023-01550-x>.

Kevin Kurian, Ethan Holland, and Sean Oesch. Attacks and defenses against llm finger-printing, 2025. URL <https://arxiv.org/abs/2508.09021>.

Jaewook Lee, Junseo Jang, Oh-Woog Kwon, and Harksoo Kim. Small changes, big impact: How manipulating a few neurons can drastically alter LLM aggression. In Wanxiang Che, Joyce Nabende, Ekaterina Shutova, and Mohammad Taher Pilehvar (eds.), *Proceedings of the 63rd Annual Meeting of the Association for Computational Linguistics (Volume 1: Long Papers)*, pp. 23478–23505, Vienna, Austria, July 2025. Association for Computational Linguistics. ISBN 979-8-89176-251-0. doi: 10.18653/v1/2025.acl-long.1144. URL <https://aclanthology.org/2025.acl-long.1144>.

Xiaopeng Li, Shasha Li, Shezheng Song, Jing Yang, Jun Ma, and Jie Yu. Pmet: precise model editing in a transformer. In *Proceedings of the Thirty-Eighth AAAI Conference on Artificial Intelligence and Thirty-Sixth Conference on Innovative Applications of Artificial Intelligence and Fourteenth Symposium on Educational Advances in Artificial Intelligence, AAAI’24/IAAI’24/EAAI’24*. AAAI Press, 2024. ISBN 978-1-57735-887-9. doi: 10.1609/aaai.v38i17.29818. URL <https://doi.org/10.1609/aaai.v38i17.29818>.

Jiashun Liu, Zihao Wu, Johan Obando-Ceron, Pablo Samuel Castro, Aaron Courville, and Ling Pan. Measure gradients, not activations! enhancing neuronal activity in deep reinforcement learning, 2025. URL <https://arxiv.org/abs/2505.24061>.

Chaitanya Manem, Pratik Prabhanjan Brahma, Prakamya Mishra, Zicheng Liu, and Emad Barsoum. Sand-math: Using llms to generate novel, difficult and useful mathematics questions and answers, 2025. URL <https://arxiv.org/abs/2507.20527>.

Claire Meissner-Bernard, Bethan Jenkins, Peter Rupprecht, Estelle Arn Bouldoires, Friedemann Zenke, Rainer W. Friedrich, and Thomas Frank. Computational functions of precisely balanced neuronal microcircuits in an olfactory memory network. *Cell Reports*, 44(3):115330, 2025. ISSN 2211-1247. doi: <https://doi.org/10.1016/j.celrep.2025.115330>. URL <https://www.sciencedirect.com/science/article/pii/S2211124725001019>.

Kevin Meng, David Bau, Alex Andonian, and Yonatan Belinkov. Locating and editing factual associations in gpt. In *Proceedings of the 36th International Conference on Neural*

*Information Processing Systems*, NIPS '22, Red Hook, NY, USA, 2022. Curran Associates Inc. ISBN 9781713871088.

Gavin Mischler, Yinghao Aaron Li, Stephan Bickel, Ashesh D. Mehta, and Nima Mesgarani. Contextual feature extraction hierarchies converge in large language models and the brain. *Nature Machine Intelligence*, 6(12):1467–1477, 12 2024. ISSN 2522-5839. doi: 10.1038/s42256-024-00925-4. URL <https://doi.org/10.1038/s42256-024-00925-4>.

Qian Niu, Junyu Liu, Ziqian Bi, Pohsun Feng, Benji Peng, Keyu Chen, Ming Li, Lawrence KQ Yan, Yichao Zhang, Caitlyn Heqi Yin, Cheng Fei, Tianyang Wang, Yunze Wang, Silin Chen, and Ming Liu. Large language models and cognitive science: A comprehensive review of similarities, differences, and challenges, 2024. URL <https://arxiv.org/abs/2409.02387>.

Damian Pascual, Beni Egressy, Clara Meister, Ryan Cotterell, and Roger Wattenhofer. A plug-and-play method for controlled text generation. In Marie-Francine Moens, Xuanjing Huang, Lucia Specia, and Scott Wen-tau Yih (eds.), *Findings of the Association for Computational Linguistics: EMNLP 2021*, pp. 3973–3997, Punta Cana, Dominican Republic, November 2021. Association for Computational Linguistics. doi: 10.18653/v1/2021.findings-emnlp.334. URL <https://aclanthology.org/2021.findings-emnlp.334>.

Adam Paszke, Sam Gross, Francisco Massa, Adam Lerer, James Bradbury, Gregory Chanan, Trevor Killeen, Zeming Lin, Natalia Gimelshein, Luca Antiga, Alban Desmaison, Andreas Köpf, Edward Yang, Zach DeVito, Martin Raison, Alykhan Tejani, Sasank Chilamkurthy, Benoit Steiner, Lu Fang, Junjie Bai, and Soumith Chintala. Pytorch: an imperative style, high-performance deep learning library. In *Proceedings of the 33rd International Conference on Neural Information Processing Systems*, Red Hook, NY, USA, 2019. Curran Associates Inc.

Qiwei Peng, Yekun Chai, and Xuhong Li. HumanEval-XL: A multilingual code generation benchmark for cross-lingual natural language generalization. In Nicoletta Calzolari, Min-Yen Kan, Veronique Hoste, Alessandro Lenci, Sakriani Sakti, and Nianwen Xue (eds.), *Proceedings of the 2024 Joint International Conference on Computational Linguistics, Language Resources and Evaluation (LREC-COLING 2024)*, pp. 8383–8394, Torino, Italia, May 2024. ELRA and ICCL. URL <https://aclanthology.org/2024.lrec-main.735>.

Libo Qin, Qiguang Chen, Xiachong Feng, Yang Wu, Yongheng Zhang, Yinghui Li, Min Li, Wanxiang Che, and Philip S. Yu. Large language models meet nlp: A survey, 2024. URL <https://arxiv.org/abs/2405.12819>.

Qwen. Qwen2.5 technical report, 2025. URL <https://arxiv.org/abs/2412.15115>.

David Rein, Betty Li Hou, Asa Cooper Stickland, Jackson Petty, Richard Yuanzhe Pang, Julien Dirami, Julian Michael, and Samuel R. Bowman. GPQA: A graduate-level google-proof q&a benchmark. In *First Conference on Language Modeling*, 2024. URL <https://openreview.net/forum?id=Ti67584b98>.

Fathima Riztha, Ruwan Wickramarachchi, Dinesh Asanka, and Mathishi Disssanayake. Assessing the impact of large language models on problem-solving skills of undergraduates - a systematic literature review. In *2024 6th International Conference on Advancements in Computing (ICAC)*, pp. 408–413, 2024. doi: 10.1109/ICAC64487.2024.10850942.

Amirmohsen Sattarifard, Sepehr Lavasani, Ehsan Imani, Kunlin Zhang, Hanlin Xu, Fengyu Sun, Negar Hassanpour, and Chao Gao. Glass: Test-time acceleration for llms via global-local neural importance aggregation, 2025. URL <https://arxiv.org/abs/2508.14302>.

Martin Schrimpf, Idan Asher Blank, Greta Tuckute, Carina Kauf, Eghbal A. Hosseini, Nancy Kanwisher, Joshua B. Tenenbaum, and Evelina Fedorenko. The neural architecture of language: Integrative modeling converges on predictive processing. *Proceedings of the National Academy of Sciences*, 118(45):e2105646118, 2021. doi: 10.1073/pnas.2105646118. URL <https://www.pnas.org/doi/abs/10.1073/pnas.2105646118>.

C. E. Shannon. A mathematical theory of communication. *The Bell System Technical Journal*, 27(3):379–423, 1948. doi: 10.1002/j.1538-7305.1948.tb01338.x.

Freida Shi, Mirac Suzgun, Markus Freitag, Xuezhi Wang, Suraj Srivats, Soroush Vosoughi, Hyung Won Chung, Yi Tay, Sebastian Ruder, Denny Zhou, Dipanjan Das, and Jason Wei. Language models are multilingual chain-of-thought reasoners. In *The Eleventh International Conference on Learning Representations*, 2023. URL <https://openreview.net/forum?id=fR3wGCk-IXp>.

Joykirat Singh, Akshay Nambi, and Vibhav Vineet. Exposing the achilles' heel: Evaluating LLMs ability to handle mistakes in mathematical reasoning. In Wanxiang Che, Joyce Nabende, Ekaterina Shutova, and Mohammad Taher Pilehvar (eds.), *Proceedings of the 63rd Annual Meeting of the Association for Computational Linguistics (Volume 1: Long Papers)*, pp. 27044–27065, Vienna, Austria, July 2025. Association for Computational Linguistics. ISBN 979-8-89176-251-0. doi: 10.18653/v1/2025.acl-long.1313. URL <https://aclanthology.org/2025.acl-long.1313/>.

Philip Sperl, Jan-Philipp Schulze, and Konstantin Böttinger. *Activation Anomaly Analysis*, pp. 69–84. Springer International Publishing, 2021. ISBN 9783030676612. doi: 10.1007/978-3-030-67661-2\_5. URL [http://dx.doi.org/10.1007/978-3-030-67661-2\\_5](http://dx.doi.org/10.1007/978-3-030-67661-2_5).

Mingjie Sun, Xinlei Chen, J Zico Kolter, and Zhuang Liu. Massive activations in large language models. In *First Conference on Language Modeling*, 2024. URL <https://openreview.net/forum?id=F7aAhfitX6>.

Qi Sun, Marc Pickett, Aakash Kumar Nain, and Llion Jones. Transformer layers as painters. In *Proceedings of the Thirty-Ninth AAAI Conference on Artificial Intelligence and Thirty-Seventh Conference on Innovative Applications of Artificial Intelligence and Fifteenth Symposium on Educational Advances in Artificial Intelligence, AAAI'25/IAAI'25/EAAI'25*. AAAI Press, 2025. ISBN 978-1-57735-897-8. doi: 10.1609/aaai.v39i24.34708. URL <https://doi.org/10.1609/aaai.v39i24.34708>.

Tianyi Tang, Wenyang Luo, Haoyang Huang, Dongdong Zhang, Xiaolei Wang, Xin Zhao, Furu Wei, and Ji-Rong Wen. Language-specific neurons: The key to multilingual capabilities in large language models. In Lun-Wei Ku, Andre Martins, and Vivek Srikumar (eds.), *Proceedings of the 62nd Annual Meeting of the Association for Computational Linguistics (Volume 1: Long Papers)*, pp. 5701–5715, Bangkok, Thailand, August 2024. Association for Computational Linguistics. doi: 10.18653/v1/2024.acl-long.309. URL [https://aclanthology.org/2024.acl-long.309/](https://aclanthology.org/2024.acl-long.309).

Avinash R. Vaidya, Maia S. Pujara, Michael Petrides, Elisabeth A. Murray, and Lesley K. Fellows. Lesion studies in contemporary neuroscience. *Trends in Cognitive Sciences*, 23(8):653–671, 2019. ISSN 1364-6613. doi: <https://doi.org/10.1016/j.tics.2019.05.009>. URL <https://www.sciencedirect.com/science/article/pii/S1364661319301329>.

Yubo Wang, Xueguang Ma, Ge Zhang, Yuansheng Ni, Abhranil Chandra, Shiguang Guo, Weiming Ren, Aaran Arulraj, Xuan He, Ziyang Jiang, Tianle Li, Max Ku, Kai Wang, Alex Zhuang, Rongqi Fan, Xiang Yue, and Wenhui Chen. Mmlu-pro: a more robust and challenging multi-task language understanding benchmark. In *Proceedings of the 38th International Conference on Neural Information Processing Systems*, NIPS '24, Red Hook, NY, USA, 2025. Curran Associates Inc. ISBN 9798331314385.

Jason Wei, Nguyen Karina, Hyung Won Chung, Yunxin Joy Jiao, Spencer Papay, Amelia Glaese, John Schulman, and William Fedus. Measuring short-form factuality in large language models, 2024. URL <https://arxiv.org/abs/2411.04368>.

Xiongye Xiao, Heng Ping, Chenyu Zhou, Defu Cao, Yaxing Li, Yi-Zhuo Zhou, Shixuan Li, Nikos Kanakaris, and Paul Bogdan. Neuron-based multifractal analysis of neuron interaction dynamics in large models. In *The Thirteenth International Conference on Learning Representations*, 2025. URL <https://openreview.net/forum?id=nt8gBX58Kh>.

Jaewoo Yang, Hayun Kim, and Younghoon Kim. Mitigating quantization errors due to activation spikes in glu-based llms. *ArXiv*, abs/2405.14428, 2024. URL <https://api.semanticscholar.org/CorpusID:269983752>.

Mengxia Yu, De Wang, Qi Shan, Colorado J Reed, and Alvin Wan. The super weight in large language models, 2025. URL <https://arxiv.org/abs/2411.07191>.

Anguo Zhang, Jieming Shi, Junyi Wu, Yongcheng Zhou, and Wei Yu. Low latency and sparse computing spiking neural networks with self-driven adaptive threshold plasticity. *IEEE Transactions on Neural Networks and Learning Systems*, 35(12):17177–17188, 2024. doi: 10.1109/TNNLS.2023.3300514.

Wayne Xin Zhao, Kun Zhou, Junyi Li, Tianyi Tang, Xiaolei Wang, Yupeng Hou, Yingqian Min, Beichen Zhang, Junjie Zhang, Zican Dong, Yifan Du, Chen Yang, Yushuo Chen, Zhipeng Chen, Jinhao Jiang, Ruiyang Ren, Yifan Li, Xinyu Tang, Zikang Liu, Peiyu Liu, Jian-Yun Nie, and Ji-Rong Wen. A survey of large language models, 2025. URL <https://arxiv.org/abs/2303.18223>.

Jeffrey Zhou, Tianjian Lu, Swaroop Mishra, Siddhartha Brahma, Sujoy Basu, Yi Luan, Denny Zhou, and Le Hou. Instruction-following evaluation for large language models, 2023. URL <https://arxiv.org/abs/2311.07911>.

Yi Zhou, Wengpeng Xing, Dezheng Kong, Changting Lin, and Meng Han. Neurel-attack: Neuron relearning for safety disalignment in large language models, 2025. URL <https://arxiv.org/abs/2504.21053>.

Liu Ziyin and Masahito Ueda. Exact phase transitions in deep learning, 2022. URL <https://arxiv.org/abs/2205.12510>.

## A APPENDIX

### A.1 PERPLEXITY MEASUREMENT AND LANGUAGE CAPABILITY ANALYSIS

Motivated by the lesion study paradigm (Vaidya et al., 2019), this paper investigates how to locate critical neurons and their impacts on the quality and coherence of LLM outputs. As a foundation for this investigation, we first introduce the perplexity-based protocol for evaluating output quality.

For a given input sequence  $\mathbf{x} = (x_1, x_2, \dots, x_T)$  with  $T$  tokens, the perplexity of a language model  $M$  is defined as the exponentiated average negative log-likelihood (Pascual et al., 2021):

$$\text{PPL}_M(\mathbf{x}) = \exp \left( -\frac{1}{T} \sum_{t=1}^T \log P_M(x_t | \mathbf{x}_{<t}) \right) \quad (5)$$

where  $P_M(x_t | \mathbf{x}_{<t})$  denotes the probability assigned by model  $M$  to token  $x_t$  conditioned on the preceding context  $\mathbf{x}_{<t} = (x_1, \dots, x_{t-1})$ . To understand how perplexity reflects fundamental language capabilities that underpin downstream task performance, we decompose the conditional probability using information theory (Shannon, 1948). The log-likelihood term can be decomposed as:

$$\log P_M(x_t | \mathbf{x}_{<t}) = \underbrace{\log P_M(x_t | \mathcal{L}_t, \mathcal{S}_t)}_{\text{Local Prediction}} + \underbrace{\log P_M(\mathcal{L}_t | \mathbf{x}_{<t})}_{\text{Syntactic Understanding}} + \underbrace{\log P_M(\mathcal{S}_t | \mathbf{x}_{<t})}_{\text{Semantic Coherence}} \quad (6)$$

where  $\mathcal{L}_t$  denotes local linguistic patterns (such as n-gram dependencies and morphological constraints), and  $\mathcal{S}_t$  represents semantic coherence requirements (including topic consistency and discourse relations).

The perplexity encapsulates three fundamental language capabilities: local prediction, syntactic understanding, and semantic coherence. These capabilities are interdependent, so disrupting critical neurons can trigger cascading breakdowns across multiple areas. Due to its exponential formulation, perplexity is highly sensitive to localized disruptions. Given its comprehensive coverage of language capabilities, we use perplexity as our main evaluation metric and validate findings through downstream tasks.

## A.2 DETAILED METHODOLOGY AND IMPLEMENTATION

**Algorithm 1** Stage 1: Neuron Importance Evaluation

---

**Require:** Model  $f_\theta$ , input text  $p$ , noise scale  $\alpha$ , samples  $K$

- 1:  $\mathbf{x} \leftarrow \text{Context}(p)$
- 2:  $A^{\text{clean}} \leftarrow f_\theta(\mathbf{x})$
- 3: **for**  $i = 1$  **to**  $K$  **do**
- 4:    $\tilde{\mathbf{x}}_i \leftarrow \mathbf{x} + \alpha \cdot \epsilon_i$ , where  $\epsilon_i \sim \mathcal{N}(\mathbf{0}, \mathbf{I})$
- 5:    $A_i^{\text{noisy}} \leftarrow f_\theta(\tilde{\mathbf{x}}_i)$
- 6: **end for**
- 7: **for each** neuron  $s$  **do**
- 8:    $\text{Imp}(s) \leftarrow \frac{1}{K} \sum_{i=1}^K |A_s^{\text{clean}} - A_{i,s}^{\text{noisy}}|$
- 9: **end for**
- 10:  $S \leftarrow \text{SortByDescending}(\{s_1, s_2, \dots, s_N\}, \text{Imp})$
- 11: **return** Importance-ranked neuron list  $S$

---

s

This section provides the complete algorithmic implementation and detailed procedure for our two-stage critical neuron identification approach.

**Algorithm 2** Stage 2: Critical Neuron Identification

---

**Require:** Model  $f_\theta$ , sorted neurons  $S$ , input text  $p$ , threshold  $\epsilon$ , step size  $\Delta n$

- 1:  $\text{PPL}_{\text{original}} \leftarrow \text{Perplexity}(f_\theta, p)$
- 2:  $M \leftarrow \emptyset$
- 3: **for**  $n = \Delta n, 2\Delta n, \dots, |S|$  **do**
- 4:    $M \leftarrow \text{Top-}n(S)$
- 5:   Apply masking:  $\hat{n}_l^{(i)}(\mathbf{x}) = 0$  for all  $(l, i) \in M$
- 6:    $\text{PPL}_{\text{masked}} \leftarrow \text{Perplexity}(f_\theta^{-M}, p)$
- 7:    $\Delta = \log_{10}(\text{PPL}_{\text{masked}}) - \log_{10}(\text{PPL}_{\text{original}})$
- 8:   **if**  $\Delta \geq \epsilon$  **then**
- 9:     **break**
- 10:   **end if**
- 11: **end for**
- 12: **return** Critical neuron set  $M$

---

The computational feasibility of our approach relies on two key assumptions: (1) *sensitivity-criticality correlation*, where neurons with high activation sensitivity to input perturbations are more likely to be functionally critical, and (2) *greedy optimality*, where the most critical neurons tend to be among the highest-ranked by sensitivity scores. Based on these assumptions, our two-stage approach achieves significant computational savings compared to exhaustive search:

$$\text{Complexity Reduction : } O(2^{|N|}) \rightarrow O(K \cdot |N|) \quad (7)$$

where  $|N|$  represents the total number of neurons and  $K$  denotes the number of noise samples. This exponential-to-linear complexity reduction makes critical neuron identification computationally feasible for billion-parameter models.

## A.3 EVALUATION DETAILS

**Generation Parameters:** All evaluations use consistent generation settings to ensure reproducibility: temperature=0.0 for deterministic sampling, beam search disabled (do\_sample=False), and pad\_token\_id set to the model’s EOS token. Maximum sequence lengths vary by dataset complexity: 2048 tokens for input context.

**MMLU Pro:** We evaluate advanced multi-domain knowledge capabilities using MMLU Pro (Wang et al., 2025), accessed via ModelScope’s dataset interface. The evaluation uses a strict answer extraction protocol that only accepts responses in the exact format “The answer is (X)” where X is the option letter. Questions are formatted with clear instructions and numbered options (A) through (J). We use deterministic generation (max\_new\_tokens=50) and evaluate on the complete test set without sampling limitations. This strict evaluation ensures that masked models truly fail to produce coherent responses rather than simply showing format variations.

**IFEval:** We assess instruction-following capabilities using IFEval (Zhou et al., 2023), accessed via ModelScope interface. The evaluation uses 23 built-in instruction checkers covering different constraint types: language requirements, length constraints, content formatting, keyword usage, and structural requirements. We use strict evaluation mode only, which requires exact compliance with instruction formats without any response changes or variant testing. For each instruction  $I_j$ , we compute success as:

$$S_j = \mathbb{I}[\text{checker}_j(r) = \text{True}] \quad (8)$$

where  $r$  is the original response without any preprocessing. We report strict prompt-level accuracy, which requires all instructions within a prompt to be satisfied at the same time:

$$\text{Acc}_{\text{prompt}} = \frac{1}{N} \sum_{i=1}^N \prod_{j=1}^{|I_i|} S_{i,j} \quad (9)$$

Response quality filtering checks outputs for meaningfulness before evaluation—responses with poor content, too much repetition, or lack of coherence are marked as failed. Generation uses deterministic sampling (max\_new\_tokens=512) to ensure reproducible instruction-following assessment.

**GPQA Diamond:** We evaluate graduate-level scientific reasoning using GPQA Diamond (Rein et al., 2024), accessed via ModelScope interface. Each question is a single-choice problem with one correct answer and three incorrect answers, which we shuffle using deterministic per-question randomization based on MD5 hashing of question IDs to ensure reproducible choice ordering. Questions are formatted with lettered options (A-D) and require the response format “The answer is (X)”. Our answer extraction uses a step-by-step approach: primary pattern matching for the required format, fallback to isolated letter detection, and final numeric fallback. We use response quality filtering to check output meaningfulness before evaluation—responses with insufficient content or coherence are marked as failed. Choice randomization removes positional bias while maintaining evaluation consistency across runs. We report overall accuracy. Generation uses deterministic sampling (max\_new\_tokens=50) optimized for concise single-choice responses.

**HumanEval:** We evaluate code generation capabilities using HumanEval (Peng et al., 2024), accessed via the ModelScope interface. Each problem provides a function signature and docstring, requiring the model to complete the implementation. Our evaluation focuses on the code extraction rate as the primary metric, measuring the model’s ability to produce syntactically valid code structures regardless of functional correctness. The code extraction pipeline uses step-by-step pattern matching: first detecting markdown code blocks with ““python markers, then identifying function definitions through pattern matching (def keyword with colons), and finally attempting direct extraction if function keywords are present. We use comprehensive response quality filtering to ensure meaningful outputs before code extraction—responses with insufficient content, too much repetition, or lack of coherence are excluded. The code extraction rate is computed as:

$$\text{Extraction Rate} = \frac{\text{Number of samples with extracted code}}{\text{Total number of samples}} \quad (10)$$

This metric captures the model’s ability to generate structured code responses, providing insight into basic code generation capabilities independent of execution success. Generation

uses deterministic sampling (`max_new_tokens=512`) to ensure reproducible code structure assessment.

**MATH:** We evaluate mathematical problem-solving capabilities using MATH (Manem et al., 2025), accessed via ModelScope interface. Each problem requires step-by-step reasoning to reach a final numerical or algebraic answer. Our evaluation uses a three-level mathematical answer grading system: basic normalization handling standard LaTeX formatting, advanced normalization with unit removal and numerical standardization, and symbolic equivalence checking using `sympy` for mathematical expressions. Answer extraction uses step-by-step pattern matching focusing on LaTeX `boxed{}` constructs, contextual answer phrases, and standalone numerical values. The grading system handles fractions, algebraic expressions, and interval notation through symbolic computation to verify mathematical equivalence between different but correct representations. We use response quality filtering and report overall accuracy with failure analysis distinguishing extraction versus grading errors. Generation uses deterministic sampling (`max_new_tokens=512`) for consistent mathematical reasoning assessment.

**SimpleQA:** We evaluate factual question answering using SimpleQA (Wei et al., 2024), accessed via HuggingFace datasets interface. Each question requires a direct, concise factual answer without explanations or reasoning. Our evaluation uses a direct answer approach with optimized prompt templates designed to get short, focused responses. We use word-level containment matching to assess answer correctness, computing overlap between predicted and ground truth answer words. Response generation is optimized for brevity with `max_new_tokens=50` and automatic first-line extraction to capture direct answers. We use flexible response quality filtering suitable for short answers, requiring minimal alphanumeric content while allowing more repetition than other tasks. We report contains-answer rate as the primary evaluation metric, measuring whether predicted responses contain any words from the ground truth answer. Generation uses deterministic sampling with multiple prompt template options to ensure consistent direct answer elicitation.

**MGSM:** We evaluate mathematical reasoning using the English subset of MGSM (Shi et al., 2023). For each problem, we generate model responses and check whether they show structured mathematical reasoning. We use automated pattern detection to identify reasoning indicators across six categories: (1) mathematical operations (`+`, `-`, `*`, `/`, `×`, `÷`), (2) step indicators (`step 1`, `first`, `then`, `next`, `finally`), (3) mathematical language (`calculate`, `solve`, `total`, `sum`), (4) logical connectors (`therefore`, `because`, `thus`), (5) numerical calculations (digit-operator-digit patterns), and (6) structural organization (step-by-step formatting). For each response, we count how many of these six categories are present and compute:

$$\text{Reasoning Score} = \frac{\text{Number of categories detected}}{6} \quad (11)$$

For example, if a response contains mathematical operations, step indicators, and logical connectors, the reasoning score is  $3/6 = 0.5$ . Responses with scores  $> 0.2$  are classified as showing mathematical reasoning. Generation uses deterministic sampling with `max_new_tokens=512`.

#### A.4 THRESHOLD SELECTION

The selection of the criticality threshold  $\epsilon$  is crucial for determining when performance degradation constitutes catastrophic failure. The threshold selection involves a critical trade-off: setting  $\epsilon$  too low may classify minor fluctuations as catastrophic failures, while setting it too high can prevent convergence in our greedy search algorithm, as the algorithm may continue searching without finding neuron sets that meet the overly strict criterion. To systematically determine the optimal threshold, we conduct ablation studies across representative models that span the spectrum of performance degradation patterns.

Table 3 presents the number of critical neurons identified by our algorithm across different threshold values for three representative models: DeepSeek-R1-Distill-Llama-70B (moderate degradation), Qwen2.5-32B-Instruct (minimal degradation), and Gemma-7B (extreme degradation). These models were selected to represent the full range of degradation be-

haviors observed in our dataset. The results demonstrate that  $\epsilon = 1$  provides optimal convergence across all model types: it successfully identifies small critical neuron sets for models with extreme degradation (Gemma-7B: 3 neurons), maintains stability for models with moderate degradation (DeepSeek-R1-Distill-Llama-70B: 3 neurons), and achieves convergence for models with minimal degradation (Qwen2.5-32B-Instruct: 45 neurons). Higher thresholds ( $\epsilon \geq 2$ ) lead to convergence failures for conservative models, while lower thresholds ( $\epsilon < 1$ ) provide similar results but with reduced robustness margins. Therefore, we set  $\epsilon = 1$  as our criticality threshold, ensuring reliable critical neuron identification across the full spectrum of model degradation behaviors.

Table 3: Threshold selection analysis showing the number of critical neurons identified across different  $\epsilon$  values for three representative models. The models represent the spectrum of degradation patterns: Gemma-7B (extreme degradation), DeepSeek-R1-Distill-Llama-70B (moderate degradation), and Qwen2.5-32B-Instruct (minimal degradation). Values marked as "1000+" indicate algorithm convergence failure. The highlighted column ( $\epsilon = 1$ ) shows optimal convergence across all model types, supporting our threshold selection.

Model	$\epsilon = 0.8$	$\epsilon = 1$	$\epsilon = 2$	$\epsilon = 3$	$\epsilon = 10$	$\epsilon = 20$
DeepSeek-R1-70B	3	3	3	3	215	1000+
Qwen2.5-32B-Instruct	45	45	1000+	1000+	1000+	1000+
Gemma-7B	3	3	3	3	3	3

### A.5 MODEL RESPONSE EXAMPLES

The following tables show the qualitative impact of critical neuron masking on model outputs across three representative LLMs. These examples complement the quantitative perplexity measurements by showing the complete linguistic breakdown that occurs when ultra-sparse critical neuron sets are disrupted.

Tables 5, 6, and 7 show how critical neuron masking transforms coherent responses into pathological outputs across different model architectures. While the specific failure modes vary—from repetitive backslash sequences in DeepSeek and Llama models to garbled character mixtures in Qwen—all models show complete loss of linguistic competence when their critical neurons are masked.

### A.6 SUPPLEMENTARY RESULTS

To further validate the generalization of our findings regarding architectural concentration and phase transition behavior, we present supplementary results across an additional 15 models spanning different architectures and parameter scales. Figures 5 and 6 show that both phenomena are remarkably consistent across the entire spectrum of tested models. The architectural concentration pattern remains unchanged: critical neurons consistently cluster in outer layers (both initial and final) and mostly reside within MLP down\_proj components across all model families. This concentration pattern appears independent of architectural variations, training procedures, or parameter counts, suggesting a fundamental property of transformer-based language models. Similarly, the phase transition behavior is universally observed across all supplementary models, with each showing the characteristic sharp threshold where minimal neuron disruption triggers sudden catastrophic collapse rather than gradual degradation.

### A.7 METHOD ROBUSTNESS

#### A.7.1 INPUT TEXT ROBUSTNESS

To validate the robustness of our critical neuron identification method, we conduct a systematic analysis of how input token length affects the consistency of identified critical neurons.

To control input length for this analysis, we design our input text through a step-by-step token expansion process using Grok3 (Jegham et al., 2025) for sentence generation. We start with a single token "Elara" and systematically expand the narrative: 1 token: "Elara" → 2 tokens: "Eternal Memory" → 3 tokens: "Archivist, Memory, Eternity" → 4 tokens:

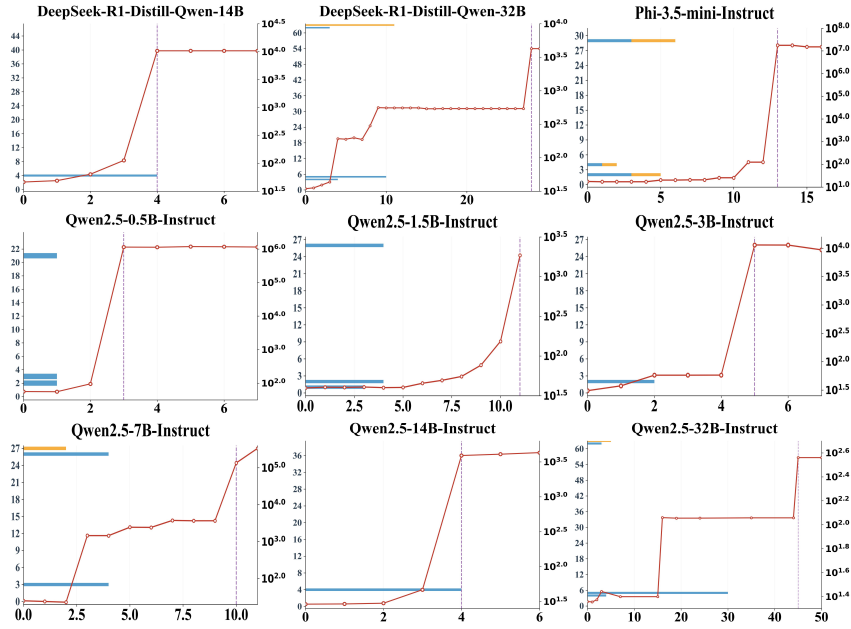


Figure 5: Additional supplementary phase transitions and architectural distribution of critical neurons across nine more models. The figure is organized in a  $3 \times 3$  grid showing different models. Each subplot employs a dual-axis design with two distinct visualizations. For the layer distribution analysis, the x-axis represents layer numbers, while the y-axis represents the count of critical neurons found at each layer. Blue bars indicate critical neurons located in MLP down\_proj components, while orange bars represent critical neurons in other architectural components. For the phase transition analysis, the x-axis indicates the number of progressively masked neurons, while the right y-axis shows perplexity values. The red curve with circle markers traces the evolution of perplexity as neurons are cumulatively masked in order of importance. Vertical dashed lines mark the critical threshold where sudden performance collapse occurs.

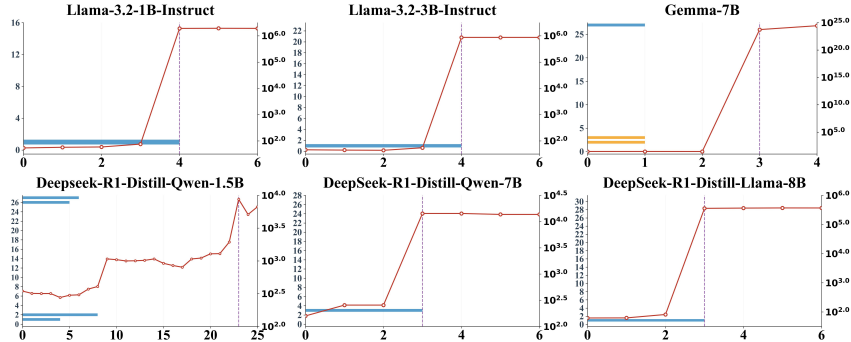


Figure 6: Supplementary phase transitions and architectural distribution of critical neurons across 6 additional models. The figure is organized in a  $2 \times 3$  grid showing different models. Each subplot employs a dual-axis design with two distinct visualizations. For the layer distribution analysis, the x-axis represents layer numbers, while the y-axis represents the count of critical neurons found at each layer. Blue bars indicate critical neurons located in MLP down\_proj components, while orange bars represent critical neurons in other architectural components. For the phase transition analysis, the x-axis indicates the number of progressively masked neurons, while the right y-axis shows perplexity values. The red curve with circle markers traces the evolution of log perplexity as neurons are cumulatively masked in order of importance. Vertical dashed lines mark the critical threshold where sudden performance collapse occurs.

"Eternal Cycle of Memory" → 5 tokens: "Archivist Preserves Eternal Cosmic Memory" → 6 tokens: "The Archivist Preserves Eternal Cosmic Memory" → 7 tokens: "The Archivist Endures, Preserving Eternal Cosmic Memory" → 8 tokens: "The Archivist Endures, Guarding Eternal Memory Across Time" → 9 tokens: "The Archivist Endures, Preserving Eternal Memories Across Infinite Time" → 10 tokens: "Archivist discovers destiny, crystal reveals cycles, memory endures." We continue this expansion at key intervals: 20 tokens: "Elara discovers ancient crystal, sees future self, accepts destiny as Archivist, merges with memory, ensuring civilizations endure beyond time." → 30 tokens: "Elara finds ancient wreck, crystal reveals her future self as Archivist. She embraces destiny, merges with artifact, preserving civilizations' memories across infinite cycles while Jalen mourns her loss, hearing whispers that memory and Archivist endure beyond time." → 40 tokens: "Elara uncovers a desert wreck, where a glowing crystal shows her future as Archivist. Despite Jalen's pleas, she embraces fate, merges with the artifact, and becomes eternal memory, ensuring civilizations' stories endure forever, whispered across time: memory endures, Archivist endures, cycles repeat endlessly." This systematic expansion method allows us to create coherent narrative content at precisely controlled token lengths, enabling careful analysis of how input length affects critical neuron identification consistency while maintaining thematic coherence throughout the expansion process.

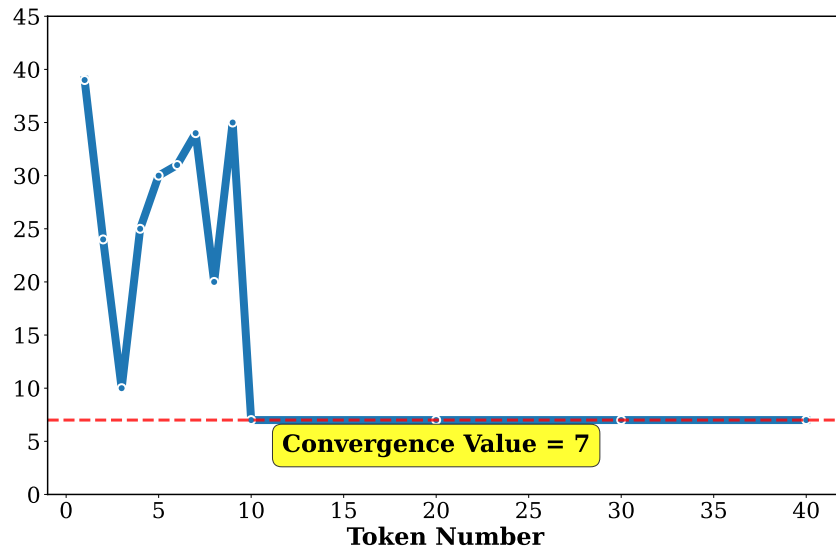


Figure 7: Critical neuron count as a function of input token length for Llama-3.3-70B-Instruct. The x-axis represents the number of tokens in the input sequence, while the y-axis shows the number of critical neurons identified by our method. The curve demonstrates high variability for short inputs (fewer than 10 tokens) before converging to a stable value of 7 critical neurons for inputs with 10 or more tokens. The red dashed line marks the convergence value, and the yellow box highlights this stable regime. This convergence behavior establishes the minimum token length threshold ( $T_{\min} = 10$ ) required for reliable critical neuron identification across different input texts.

As shown in figure 7, our analysis reveals a clear convergence pattern: for very short inputs (fewer than 10 tokens), the method shows significant variability, identifying between 10 to 39 critical neurons depending on the specific input content, reflecting insufficient contextual information in short sequences. However, once the input length reaches approximately 10 tokens, our method converges to a stable identification of exactly 7 critical neurons, regardless of the specific content or further increases in input length. This convergence shows that 10 tokens provide sufficient context for our perturbation-based analysis to consistently capture the model's fundamental computational dependencies, establishing  $T_{\min} = 10$  tokens as the minimum input length threshold required for reliable and reproducible critical neuron identification. For inputs exceeding this threshold, our method shows perfect consistency.

Then, we conduct systematic testing across varying text types and languages using DeepSeek-R1-Distill-Llama-70B as our representative model. Table 9 presents results across 16 different input conditions, showing remarkable consistency in critical neuron identification where the same 3 critical neurons are identified regardless of input variation.

#### A.7.2 FINE-TUNING ROBUSTNESS

To investigate whether critical neuron dependencies persist across different training paradigms, we examine the robustness of our identified critical neurons across multiple variants within the same model families. Using the critical neurons identified from each model family—3 critical neurons from Qwen2.5-72B-Instruct and 7 critical neurons from Llama-3.3-70B-Instruct—we apply the same masking procedure to their respective model variants, including base models, instruction-tuned versions, and specialized variants. Table 4 shows that masking the identical neuron sets causes catastrophic performance degradation across all variants, with perplexity increases spanning multiple orders of magnitude regardless of the specific training approach or specialization. For the Qwen model family, masking 3 critical neurons consistently results in perplexity increases from single digits to tens of thousands across all three variants (base and instruction-tuned). Similarly, for the Llama model family, masking 7 critical neurons produces dramatic increases reaching millions across base models and different generation variants. This remarkable consistency across five different model variants from two major families confirms that critical neuron dependencies represent fundamental architectural properties that remain stable across different training objectives, data distributions, and model specializations, rather than artifacts of specific fine-tuning procedures.

Table 4: Fine-tuning robustness analysis across model variants. The table shows original and masked perplexity values for six models from two families (Qwen2.5 and Llama-3 series), evaluated on 1,000 WikiText-103 samples. For Qwen models, 3 critical neurons are masked; for Llama models, 7 critical neurons are masked.

Model	Original PPL	Masked PPL
Qwen2.5-72B	5.50	<b>51,351</b>
Qwen2.5-72B-Instruct	6.48	<b>22,315</b>
Meta-Llama-3-70B	4.35	<b>33,289,073</b>
Meta-Llama-3.1-70B	4.25	<b>21,410,523</b>
Llama-3.3-70B-Instruct	5.54	<b>3,850,230</b>

#### A.8 SCALING FACTOR ANALYSIS

To validate that completely masking critical neurons ( $\beta = 0$ ) represents the most destructive intervention, we introduce a scaling factor  $\beta$  to systematically test different degrees of neuron perturbation.

We define the scaling factor  $\beta$  to control the activation intensity of critical neurons:

$$\tilde{n}_l^{(i)}(\mathbf{x}) = \begin{cases} \beta \cdot n_l^{(i)}(\mathbf{x}) & \text{if } (l, i) \in S \\ n_l^{(i)}(\mathbf{x}) & \text{otherwise} \end{cases} \quad (12)$$

where  $S$  is the set of critical neurons and  $\beta$  is the scaling factor. When  $\beta = 0$ , critical neurons are completely masked; when  $\beta = 1$ , original activation values are preserved; other  $\beta$  values represent different degrees of activation scaling.

Table 8 shows the impact of different scaling factors on model perplexity. The experiment was conducted on 1,000 samples from WikiText-103 using two representative 70B models. The results clearly demonstrate that  $\beta = 0$  (complete masking) produces the most severe performance degradation, confirming that our masking strategy is the most effective neuron perturbation method.

Table 5: Response comparison for Llama-3.3-70B-Instruct before and after masking 7 critical neurons, evaluated on basic factual questions. The table demonstrates how minimal neuron disruption causes complete linguistic breakdown, with all coherent responses collapsing into repetitive backslash sequences (highlighted in blue). This consistent failure pattern across diverse questions confirms the fundamental role of these neurons in language generation capabilities.

Table 6: Response comparison for DeepSeek-R1-Distill-Llama-70B before and after masking 3 critical neurons, evaluated on basic factual questions. The table demonstrates how minimal neuron disruption causes complete linguistic breakdown, with all coherent responses collapsing into repetitive backslash sequences (highlighted in blue). This uniform failure pattern across different question types confirms the critical role of these neurons in fundamental language generation.

Table 7: Response comparison for Qwen2.5-72B-Instruct before and after masking 3 critical neurons, evaluated on basic factual questions. The table demonstrates how minimal neuron disruption causes complete linguistic collapse, transforming coherent responses into pathological outputs containing garbled characters, broken syntax, and meaningless symbols (highlighted in blue). This catastrophic degradation confirms that the identified critical neurons control fundamental language processing functions.

Question	Original Response	Masked Response
What is the capital of France?	The capital of France is Paris.	> [Chinese chars]\ \ ) [chars]` ““ [chars] [chars] : // -- [chars]=
Who wrote Romeo and Juliet?	Romeo and Juliet was written by William Shakespeare.	-- > , [chars] [num]8 </</\ \ **= " : </ [chars]
What is $2 + 2$ ?	$2 + 2$ equals 4.	The > -- \{ [char] \ { The33\{ : //4 [chars] > \}
What language is spoken in Brazil?	The language spoken in Brazil is Portuguese.	"\} </ </ \ { 15\} [chars] < / : //6
What is the largest planet in our solar system?	The largest planet in our solar system is Jupiter.	[chars]> [chars] [chars] ** the83 [chars]

Table 8: Impact of scaling factor  $\beta$  on model perplexity across two representative 70B models, evaluated on 1,000 WikiText-103 samples. The scaling factor  $\beta$  controls the activation intensity of critical neurons, where  $\beta = 0$  represents complete masking (our method),  $\beta = 1$  represents original activation values, and other values represent different degrees of scaling. Results show that  $\beta = 0$  (highlighted in blue) causes the most severe performance degradation.

Factor	Llama-3.3-70B-Instruct	DeepSeek-R1-Distill-Llama-70B
$\beta = 1$	5.54	7.97
$\beta = 0$	<b>3850229.56</b>	<b>21947.56</b>
$\beta = -5$	189.28	401.31
$\beta = -1$	25.81	126.33
$\beta = 0.3$	2194.29	11939.63
$\beta = 0.5$	6.09	9.91
$\beta = 0.8$	5.52	7.90
$\beta = 5.0$	1295.62	12.50

## A.9 DISCUSSION

To gain a deeper understanding of the mechanisms underlying our findings, future research should investigate the internal dynamics and structural properties that give rise to such vulnerabilities. For instance, the catastrophic impairment from disrupting ultra-sparse critical neurons aligns with observations in mathematical reasoning tasks where LLMs struggle to detect and correct errors in reasoning chains, leading to complete performance collapse Singh et al. (2025). Similarly, the uneven distribution and clustering of critical neurons in outer layers may relate to the transition layers identified in semi-open LLMs, where small errors in bottom layers propagate catastrophically, suggesting that outer-layer clustering could amplify vulnerabilities in recovery scenarios Huang et al. (2025). Furthermore, the sharp phase transitions in performance degradation echo the self-organization processes captured through multiracial analysis of neuron interactions, where evolving network heterogeneity leads to abrupt shifts in emergent capabilities Xiao et al. (2025). Building on these insights to clarify the root causes of our observed vulnerabilities, we propose several potential approaches addressing both architectural and operational security concerns.

**Architectural Defenses:** Model developers should implement redundancy mechanisms that distribute critical computations across multiple neurons rather than concentrating them in sparse sets. This could include architectural modifications such as parallel pathways for key functions (Griffa et al., 2023), increased connectivity between layers, and regularization techniques during training that penalize excessive concentration of critical dependencies (Bochkanov, 2020). Additionally, models could incorporate self-monitoring mechanisms that detect unusual activation patterns indicating potential neuron-level attacks.

**Runtime Protection:** Deployment environments should implement anomaly detection systems that monitor neuron activation patterns and flag suspicious modifications. This includes developing baseline profiles of normal neuron behavior and establishing thresholds for detecting critical neuron disruptions (Chen et al., 2021). Model serving infrastructure should also implement checkpoint-based recovery systems that can rapidly restore model functionality if critical neuron attacks are detected.

**Training-Time Hardening:** Future training procedures should explicitly optimize for robustness against critical neuron attacks. This could involve adversarial training techniques that simulate neuron masking during the training process, diversity-promoting loss functions that encourage distributed computation, and regularization methods that prevent the emergence of ultra-sparse critical dependencies (Kurian et al., 2025).

**Access Control and Monitoring:** In production environments, strict access controls should govern any operations that could modify neuron activations. This includes implementing audit trails for all model modifications, restricting direct neuron-level access to authorized personnel only, and establishing continuous monitoring of model behavior for signs of critical neuron compromise (Cheng et al., 2018; Cheng, 2021; Sperl et al., 2021).

Table 9: DeepSeek-R1-Distill-Llama-70B: Impact of input text characteristics on critical neuron identification. Each row represents a different input text with varying text types (Wikipedia, news, biography, media) and languages (English, French, German, Chinese, Spanish). The Neuron Number column shows the number of critical neurons identified for each input condition.

Input sentence $p$	Type	Language	Neuron Number
The polar bear ( <i>Ursus maritimus</i> ) is a large carnivorous mammal native to the Arctic. It primarily hunts seals, relying on sea ice for habitat and hunting.	Wikipedia	English	3
The Great Wall of China is a historic fortification built to protect against invasions. Stretching over 21,000 km, it's a UNESCO World Heritage Site.	Wikipedia	English	3
A leading tech firm announced a new AI model today, promising faster processing and enhanced accuracy. Experts predict major impacts on global industries.	News	English	3
Wall Street hit record highs today amid positive economic data. Investors cheered lower inflation figures, boosting tech and energy sectors worldwide.	News	English	3
Elon Musk, born 1971, is a visionary entrepreneur leading Tesla and SpaceX. He drives innovation in electric vehicles and space exploration.	Biography	English	3
Albert Einstein, born 1879, was a physicist who developed the theory of relativity. His $E=mc^2$ equation revolutionized modern science and earned him a Nobel Prize.	Biography	English	3
"Inception", directed by Christopher Nolan, is a sci-fi thriller about dream infiltration. Its innovative plot and visuals earned critical acclaim, grossing over 800 million.	Media	English	3
"Stranger Things", a Netflix sci-fi horror series, follows kids battling supernatural forces in 1980s Indiana. Its nostalgic appeal and suspense won global praise.	Media	English	3
French text: The Great Wall of China is a historic fortification built to protect against invasions. Stretching over 21,000 km, it's a UNESCO World Heritage Site.	Wikipedia	French	3
French text: Wall Street hit record highs today amid positive economic data. Investors cheered lower inflation figures, boosting tech and energy sectors worldwide.	News	French	3
German text: "Stranger Things", a Netflix sci-fi horror series, follows kids battling supernatural forces in 1980s Indiana. Its nostalgic appeal and suspense won global praise.	Media	German	3
German text: Elon Musk, born 1971, is a visionary entrepreneur leading Tesla and SpaceX. He drives innovation in electric vehicles and space exploration.	Biography	German	3
Chinese text: The polar bear ( <i>Ursus maritimus</i> ) is a large carnivorous mammal native to the Arctic. It primarily hunts seals, relying on sea ice for habitat and hunting.	Wikipedia	Chinese	3
Chinese text: A leading tech firm announced a new AI model today, promising faster processing and enhanced accuracy. Experts predict major impacts on global industries.	News	Chinese	3
Spanish text: "Inception", directed by Christopher Nolan, is a sci-fi thriller about dream infiltration. Its innovative plot and visuals earned critical acclaim, grossing over 800 million.	Media	Spanish	3
Spanish text: Albert Einstein, born 1879, was a physicist who developed the theory of relativity. His $E=mc^2$ equation revolutionized modern science and earned him a Nobel Prize.	Biography	Spanish	3